

A quantitative interpretation of the coefficients in Figs. 26 and 27 should be approached with some caution. Near the ρ^0 mass A_2/A_0 has a maximum value of 1.3 instead of 2.0 as expected for pure P -wave scattering.¹⁷ This indicates the importance of absorption effects. Furthermore, in the same mass region A_2/A_0 for $\pi^0\pi^-$ is roughly a factor of 2 smaller than for $\pi^+\pi^-$. This discrepancy seems to be due to vector exchange in ρ^- production which is significant¹⁸ near 4 GeV/c. It was pointed out above that an expansion of the angular

distribution in powers of $\cos\theta_{\pi\pi}$, Eq. (7), proved particularly useful for phase-shift calculations because the ratio b/c was found to be independent of t . The terms in expression (12) are found to be strongly t -dependent. In Fig. 28 we show the results of extrapolating the Legendre coefficients A_1/A_0 and A_2/A_0 to the pion pole. The curves are least-squares fits to a quadratic form in t . Both coefficients are seen to depend strongly on t and the values at the pole have large errors associated with them.

We suggest that it is highly desirable to extend S -wave $\pi\pi$ phase-shift calculations to dipion masses greater than 900 MeV. A phase-shift analysis offers the best means of settling questions about possible resonances between the ρ^0 and f^0 . Also, it would help determine which of sets I and II is the correct set for δ_0^0 since set I approaches 180° and set II is near 90° at 900 MeV.

¹⁷ For P -wave and S -wave amplitudes

$$A_2/A_0 = 6 \sin^2\delta_1^1 / [(4/9) \sin^2\delta_0^0 + 3 \sin^2\delta_1^1].$$

If $\delta_0^0 = \frac{1}{2}\pi$ when $\delta_1^1 = \frac{1}{2}\pi$, then $A_2/A_0 = 1.74$.

¹⁸ W. L. Yen, R. L. Eisner, L. Gutay, P. B. Johnson, P. R. Klein, R. E. Peters, R. J. Sahni, and G. W. Tauffest, *Phys. Rev. Letters* **18**, 1091 (1967); I. Derado, J. A. Poirier, N. N. Biswas, N. M. Cason, V. P. Kenney, and W. D. Shephard, *Phys. Letters* **24B**, 112 (1967).

Experimental Tests of Cascade Theory at High Energies*

R. HOLYNSKI† AND W. V. JONES‡

Department of Physics and Astronomy, Louisiana State University, Baton Rouge, Louisiana 70803

AND

K. PINKAU

Max-Planck-Institut für Extraterrestrische Physik, Garching bei München, Germany

(Received 1 July 1968)

Results of simultaneous measurement of the radial position and angular orientation of electrons in ten high-energy (180–2000-BeV) electromagnetic cascades are given. Six of these cascades were developed in pure emulsion, while four were developed in a lead-emulsion sandwich stack. Numerical calculations of the angular distributions, both within approximation B and the core approximation, are presented. Calculations on the mixed radial-angular distribution are related to the separate distributions. A method is given for the use of the mixed distribution to extend the effective radial range of measurement to such an extent that the transition of the experimental results from the core approximation to approximation B becomes evident. Limited experimental verification of the often-used approximation B is thereby established. It is further shown that cascade theory is internally consistent within the region of validity of the core approximation and that the radial range must extend up to $\sim 10^{-1}$ radiation length in order to include all particles having angles as small as ~ 4 –5 deg.

I. INTRODUCTION

THE measurement of the lateral distribution of cascade electrons offers one of the few possibilities to measure the energy of ultrahigh-energy particles ($\geq 10^{11}$ eV). Such measurements rely on the experimental determination of the radial distribution of the

cascade electrons at specified distances from the cascade origin.¹ The experimental results are then compared with the theoretical calculation of the integral radial distribution in the three-dimensional cascade theory.² These theoretical calculations utilize an approximation which requires that the radius R be small compared to unity when expressed in units of the radiation length (r.l.). This is called the “core approximation”³ since it is valid only near the core of a cascade.

Experimental evidence, which has been obtained from scattering measurements on individual cascade

* Work supported by the National Science Foundation.

† On leave of absence from Institute of Nuclear Research in Krakow, Poland.

‡ Submitted in partial fulfillment of the Ph.D. degree at Louisiana State University, Baton Rouge, La. W. V. J. would like to express his appreciation for an NDEA Graduate Fellowship at Louisiana State University, and he would also like to thank the Alexander von Humboldt Stiftung in Germany for a research stipend at the Max-Planck-Institut für Extraterrestrische Physik, Garching bei München, Germany.

¹ K. Pinkau, *Phil. Mag.* **2**, 1389 (1957).

² K. Kamata and J. Nishimura, *Progr. Theoret. Phys. (Kyoto) Suppl.* **6**, 93 (1958).

³ K. Pinkau, *Nuovo Cimento* **33**, 221 (1964).

electrons⁴⁻⁶ and from the angular divergence of γ rays in the decay of π^0 mesons, seems to support the use of the core approximation up to distances of $\lesssim 10^{-2}$ r.l. from the cascade axis. However, this radial distance is near the point where the core approximation has been predicted to begin to deviate from the true electron distribution.³

One of the main objectives of this work is to find the experimental radial distribution of cascade particles up to a significantly greater distance from the axis than has previously been reported in order to check the core approximation. It should be emphasized that in obtaining the experimental distributions up to the larger distances, the core approximation is accepted as being valid up to its proven range of validity (10^{-2} r.l.), and is used up to this distance to determine the primary energy E_0 of the measured cascades. Any deviation from the core approximation can then be found by comparing the experimental distributions $N(<R)$ versus E_0R , up to the maximum distances of R which are measured, with the theoretical curves predicted by the core approximation.

Theoretically, at large R , a transition of the cascade distribution curves from the region of validity of the core approximation to the region of validity of approximation B occurs. The shape of the distribution predicted by approximation B should be independent of primary energy and should yield information on the total number of particles at any depth. Determination of the angular and radial distributions at sufficiently large distances from the cascade axis would therefore be a check on the validity of approximation B.

The experimental angular distribution of the particles in ultrahigh-energy electromagnetic cascades have not previously been measured. Because of the relation between the radial and angular coordinates, it is possible, in principle, to check any deviation of the experimental radial distribution from the core-approximation curves by using the angular distribution. Since the radius r and angle θ of a particle in a cascade are typically related by

$$\theta = r/1 \text{ r.l.},$$

the angular distribution that can be measured in emulsions covers a different (larger) domain of the variable and thus shows a more pronounced deviation from the core approximation than the radial distribution.

The angular distribution is distinct from the radial distribution in that it is insensitive to the particular geometrical arrangement of the cascade-producing material. If, for example, the cascade-producing material

is arranged in layers, the angular distribution of the cascade particles at any point will depend only on the distance from the cascade origin expressed in radiation lengths. However, the radial distribution, which is a result of the scattering process and diffusion under the angle attained in the scattering process, is dependent on the arrangement of the absorber. This is clear because the particles will diffuse outward in any less dense material or space between the production layers.

Most detectors⁷⁻⁹ employed in investigations involving measurements of high-energy electromagnetic cascades have consisted of alternate layers of lead or tungsten and nuclear emulsion. Such stacks are called "sandwich stacks." The question has remained open whether the layers of the arrangements were sufficiently small compared to the radiation length so that the absorber could be treated as a homogeneous medium. Obviously, a comparison of the angular distribution (which is not dependent on the arrangement) and the radial distribution (which is dependent on the arrangement) with each other and with the corresponding theories should reveal any inconsistencies.

In complete analogy to energy determinations from the radial distribution, the primary energy E_0 of an electromagnetic cascade can be determined from its angular distribution. The theoretical angular distributions $N(<\Theta)$ versus $E_0 \tan\Theta$ have been calculated by the authors and are presented in Sec. II B for several distances t from the cascade origin. The value of E_0 can be obtained by comparing the experimental distribution $N(<\Theta)$ versus $\tan\Theta$ with the theoretical distribution $N(<\Theta)$ versus $E_0 \tan\Theta$ in exactly the same manner as is done for the radial distribution.¹ By using the value E_0 obtained from the angular distribution, the effective radiation length of a sandwich stack having any particular geometrical arrangement can then be found by fitting the theoretical distribution $N(<R)$ versus E_0R , where R is expressed in radiation lengths, to the experimental distribution $N(<R)$ versus R with R expressed in microns. Since E_0 is known from the angular distribution, the number of microns per radiation length can be determined.

From the considerations given above, it appears to be of great importance to measure simultaneously the positions and angles of electrons in high-energy electromagnetic cascades which are observed in pure emulsion blocks and in lead-emulsion sandwich stacks that have been exposed to the cosmic radiation.

The radial and angular distributions of six electro-

⁷ J. G. Duthie, C. M. Fisher, P. H. Fowler, A. Kaddousa, D. H. Perkins, K. Pinkau, and W. Wolter, *Phil. Mag.* **6**, 89 (1961); **6**, 113 (1961).

⁸ P. K. Malhotra, P. G. Shukla, S. A. Stephens, B. Vijaylakshmi, J. Boulton, M. G. Bowler, P. H. Fowler, H. L. Kackforth, J. Keeretaavep, V. M. Mayes, and S. N. Tovey, *Nuovo Cimento* **40A**, 385 (1965).

⁹ M. Akashi, Z. Watanabe, A. Misaki, I. Mito, Y. Oyama, S. Tokunaga, T. Ogata, Y. Tsuneoka, S. Dake, K. Yokoi, S. Hasegawa, J. Nishimura, K. Niu, T. Taira, A. Nishio, T. Fujimoto, and N. Ogita, *Progr. Theoret. Phys. (Kyoto) Suppl.* **32**, 1 (1964).

⁴ K. Pinkau, *Nuovo Cimento* **3**, 1285 (1956).

⁵ O. Minakawa, Y. Nishimura, M. Tsuzuki, H. Yamanouchi, Y. Fujimoto, S. Hasegawa, J. Nishimura, and K. Niu, *Nuovo Cimento Suppl.* **11**, 125 (1959).

⁶ P. H. Fowler, D. H. Perkins, and K. Pinkau, in *Proceedings of the Moscow Cosmic Ray Conference, 1959*, edited by V. I. Zatsepin and B. A. Khrenov, (International Union of Pure and Applied Physics, Moscow, 1960), Vol. 2, p. 302.

magnetic cascades from a pure emulsion stack having energies in the range 845–2000 BeV have been measured. The same distributions have been measured for four cascades from a mixed lead-emulsion stack in the energy range 178–720 BeV.

The measurements were performed over lateral distances that permit a direct check of the core approximation up to distances seven times larger than has been previously reported. By making use of the calculations presented in Sec. II C, which relate the mixed radial-angular distributions to the separate radial and angular distributions, it is possible to check the core approximation up to even larger distances. The related problem of the transition of the actual cascade distribution from the predictions of the core approximation to approximation B, and indeed the validity of approximation B itself, also can be investigated within the range of our measurements and calculations.

The simultaneous measurements of radii and angles of the cascade particles provide a check on the internal consistency of the cascade theory within the core approximation and give the possibility for establishing the effective radiation length for the lead-emulsion sandwich stack. Furthermore, one can obtain results about the mixed radial-angular distributions which are not presently known either theoretically or experimentally.

II. THEORETICAL CALCULATIONS

A. Angular Distribution of Cascade Electrons within Approximation B

The theoretical predictions for the angular distribution of cascade electrons exist simultaneously with the predictions for the radial distributions in the three-dimensional cascade theory. However, because of previous lack of interest in making experimental angular measurements on the cascade electrons, no numerical results from the theory are presently available. Therefore it is necessary to derive the numbers predicted by the theory so that a comparison can be made with experimental results.

The normalized (to unity) number of cascade electrons having angle less than Θ with respect to the cascade axis is given by

$$N_0(<\Theta) = \int_0^\Theta P_{\pi 1}(E_0, 0, \theta, t) 2\pi\theta d\theta, \quad (1)$$

where $P_{\pi 1}(E_0, 0, \theta, t)$ is the normalized structure function for the angular distribution of electrons in the three-dimensional cascade theory of Kamata and Nishimura.² This function, which is valid for $E_0 \gg \epsilon$, can be obtained by letting $r \rightarrow \theta$ in their Eq. (3.54), and is given by

$$P_{\pi 1}(E_0, 0, \theta, t) = [2\pi^2 i \Gamma(s) M_1(0, -s, s, t)]^{-1} \times \int_{-i\infty}^{+i\infty} d\bar{p} \left(\frac{\epsilon}{E_s}\right)^2 \left(\frac{\epsilon^2 \theta^2}{E_s^2}\right)^{-\bar{p}-1} \Gamma(\bar{p}+1) \Gamma(s+2\bar{p}) \times M_1(\bar{p}, -s-2\bar{p}, s, t). \quad (2)$$

The integration over θ can be performed for negative values of the real part of \bar{p} to obtain

$$N_0(<\Theta) = [\pi i \Gamma(s) M_1(0, -s, s, t)]^{-1} \int_{-i\infty}^{+i\infty} d\bar{p} \left(\frac{\epsilon\theta}{E_s}\right)^{-2\bar{p}} \times \left(\frac{1}{-2\bar{p}}\right) \Gamma(\bar{p}+1) \Gamma(s+2\bar{p}) M_1(\bar{p}, -s-2\bar{p}, s, t). \quad (3)$$

Using the saddle-point method of solution, the integral over \bar{p} gives

$$N_0(<\Theta) = \frac{\Gamma(\bar{p}+1) \Gamma(s+2\bar{p})}{\Gamma(s)} \left(\frac{\epsilon\theta}{E_s}\right)^{-2\bar{p}} \left(\frac{1}{-\bar{p}}\right) \times [2\pi u''(\bar{p})]^{-1/2} \frac{M_1(\bar{p}, -s-2\bar{p}, s, t)}{M_1(0, -s, s, t)}, \quad (4)$$

where \bar{p} is the value of \bar{p} at the saddle point [i.e., the value of \bar{p} which maximizes the logarithm of the integrand in Eq. (3)] and is defined by

$$-2 \ln \frac{\epsilon\theta}{E_s} - \frac{1}{\bar{p}} + \psi(\bar{p}+1) + 2\psi(s+2\bar{p}) = 0. \quad (5)$$

The expression $u''(\bar{p})$ is the second-order derivative with respect to \bar{p} of the logarithm of the integrand in Eq. (3) and is given by

$$u''(\bar{p}) = (1/\bar{p}^2) + \psi'(\bar{p}+1) + 4\psi'(s+2\bar{p}). \quad (6)$$

The functions ψ and ψ' are, respectively, the first- and second-order logarithmic derivatives of the γ function and are tabulated in the literature.¹⁰

For practical application, it is sufficient to write the angular Mellin function as

$$M_1(\bar{p}, q, s, t) = m_1(\bar{p}, q, s) e^{\lambda_1(\bar{p})t}, \quad (7)$$

since $M_1(\bar{p}, q, s, t)$ is a linear function of $e^{\lambda_1(\bar{p})t}$, $e^{\lambda_1(\bar{p}+1)t}$, \dots , $e^{\lambda_2(\bar{p})t}$, $e^{\lambda_2(\bar{p}+1)t}$, \dots , and since

$$e^{\lambda_1(\bar{p})t} \gg e^{\lambda_2(\bar{p})t}, \quad e^{\lambda_1(\bar{p})t} \gg e^{\lambda_1(\bar{p}+1)t}.$$

Therefore, the recurrence relation for the angular Mellin function given by Eq. (3.33) of Ref. 2 can be expressed as

$$\{\lambda_1^2(s) + [A(s+2\bar{p}+q) + \sigma_0] \lambda_1(s) + A(s+2\bar{p}+q)\sigma_0 - B(s+2\bar{p}+q)C(s+2\bar{p}+q)\} m_1(\bar{p}, q, s) = (\lambda_1(s) + \sigma_0) \times [\bar{p} m_1(\bar{p}-1, q, s) + (s+2\bar{p}+q) q m_1(\bar{p}, q-1, s)], \quad (8)$$

with the boundary condition for an electron-pair primary being¹¹

$$m_1(0, 0, s) = B(s) H_1(s) / \sigma_0. \quad (9)$$

¹⁰ See, for example, *Handbook of Mathematical Functions*, edited by M. Abramowitz and I. A. Stegun (Dover Publications, Inc., New York, 1965), p. 255.

¹¹ J. M. Kidd, *Nuovo Cimento* 27, 57 (1963).

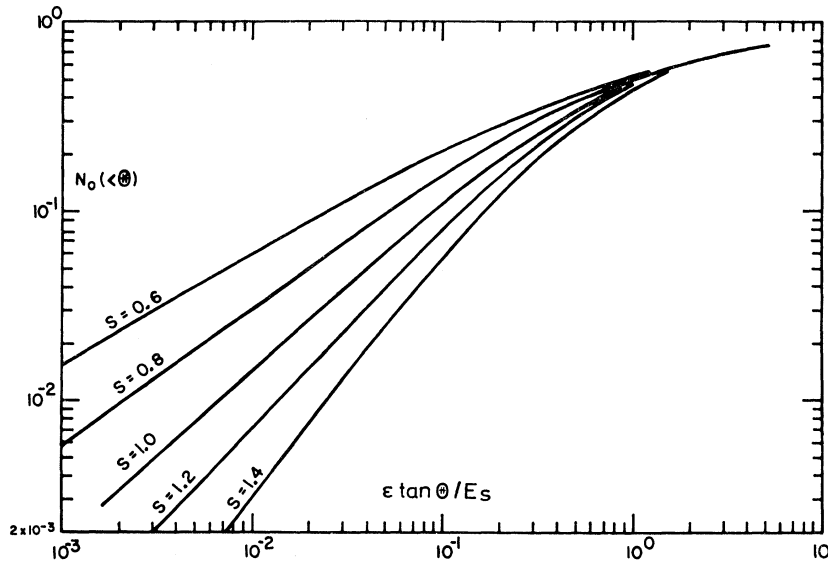


FIG. 1. Normalized integral angular distribution of cascade electrons in approximation B. The parameter s is the shower age, ϵ is the critical energy, $E_s = 21$ MeV is the scattering energy.

The tabulated values¹² of $A(s)$, $B(s)$, $C(s)$, $H_1(s)$, and $\lambda_1(s)$ can be used with this boundary condition to solve the recurrence relation for $m_1(p, q, s)$ for any positive value of p and q . However, $m_1(p, q, s)$ is needed for negative values of p since the values of θ in Eq. (4) range from 0 to ∞ as \bar{p} goes from $-\frac{1}{2}s$ to 0. Using the fact that $m_1(p, 0, s)$ has a pole at $p = -\frac{1}{2}s - 1$ (see Ref. 2), it is possible to obtain $m_1(p, 0, s)$ for negative values of p by making an extrapolation to this pole. A consistency check on this extrapolation can be made by using the recurrence relation for $m_1(p, q, s)$ for values of $q \neq 0$. In this manner, it is possible to find $m_1(p, q, s)$ for the needed values of p and q , i.e., $m_1(p, q = -s - 2p, s)$ can be found for $-\frac{1}{2}s < p \leq 0$.

By solving Eq. (5) for various values of p at fixed values of the shower-age parameter s , the normalized number of cascade particles $N_0(< \Theta)$ as a function of $\epsilon \tan \Theta / E_s$ can be obtained from Eq. (4) for each value of s . This dependence is plotted in Fig. 1 for a few values of s .

To get the distribution of cascade particles in approximation B, one must determine the correct value of t , for specific values of s and the ratio E_0/ϵ , from³

$$\ln(E_0/\epsilon) + \lambda'_1(s)t = 0. \tag{10}$$

The normalized number of particles $N_0(< \Theta)$ given in Fig. 1 must then be multiplied by the total number of particles at a fixed t and for a fixed ratio of E_0/ϵ which is given by Fig. 5.13.3 in Ref. 12.

B. Angular Distribution of Cascade Electrons within the Core Approximation

The expressions to be evaluated in obtaining the angular distribution within the core approximation are

¹² B. Rossi, *High Energy Particles* (Prentice-Hall, Inc., Englewood Cliffs, N. J., 1952).

obtained by letting $r \rightarrow \theta$ in Eqs. (6.1) and (6.2) of Kamata and Nishimura.² These equations are the series solution to the three-dimensional cascade theory without the Landau approximation. The first term in the series represents the spread caused by multiple scattering of electrons when they are traversing matter and in fact is quite similar to the solution derived under the Landau approximation. The second term of the series gives the contribution of single scattering and some of the plural scattering. Thus, this second term gives little contribution to the structure function near the shower axis but is predominant at the tail of the structure function.

The total number of particles $N(< \Theta)$ which make angles less than Θ with respect to the cascade axis for the approximation $\epsilon \theta / K \ll 1$ (core approximation) is expressed by

$$N(< \Theta) = \frac{1}{2\pi i} \int_{-i\infty}^{+i\infty} ds \left(\frac{E_0 \Theta}{K}\right)^s \left(\frac{1}{s}\right) (1 - \frac{1}{2}s) \times m_1(-\frac{1}{2}s, 0, s) e^{\lambda_1(s)t} \tag{11}$$

TABLE I. Number of electrons having angle less than Θ for electron-pair primary.

$E_0 \tan \Theta$ (BeV) \ t (r.l.)	4	5	6	7	8	9
5×10^{-1}	5.1	4.0	2.8
2×10^0	10.2	9.2	7.2	4.5
2×10^0	19.5	19.2	16.5	13.0	9.4	5.4
5×10^0	42	46	44	40	34	23
1×10^1	72	85	88	83	73	58
2×10^1	115	146	165	169	155	132
5×10^1	202	281	360	398	392	370
1×10^2	297	439	620	722	762	758
2×10^2	1015	1290	1425	1460
5×10^2	2590	3070	3400

if only the first term of the series solution is considered. The parameter K is correlated to the scattering energy E_s , and the other symbols used are the same as those described in Sec. II A. This equation can be solved by the saddle point method to give

$$N(<\Theta) = [2\pi u''(\bar{s})]^{-1/2} (E_0\Theta/K)^{\bar{s}} (1/\bar{s}) \Gamma(1-\frac{1}{2}\bar{s}) \times m_1(-\frac{1}{2}\bar{s}, 0, \bar{s}) e^{\lambda_1(\bar{s})t}, \quad (12)$$

where

$$\ln(E_0\Theta/K) - 1/\bar{s} - \frac{1}{2}\psi(1-\frac{1}{2}\bar{s}) + \lambda_1'(\bar{s})t = 0, \quad (13)$$

and

$$u''(\bar{s}) = 1/\bar{s}^2 + \frac{1}{4}\psi'(1-\frac{1}{2}\bar{s}) + \lambda_1''(\bar{s})t. \quad (14)$$

The solutions of these equations for an electron-pair primary are given in Table I and in Fig. 2 at a few values of t for $K=19.3$ MeV. The details of obtaining the Mellin function $m_1(-\frac{1}{2}\bar{s}, 0, \bar{s})$ are given in Sec. II A.

C. Mixed Radial-Angular Distribution

Cascade theory does not solve the problem of the angular distribution of cascade particles as a function of radius or of the radial distribution as a function of angle, i.e., the mixed radial-angular distributions. Rather the angular distribution considered there is the one integrated over all radii, and the radial distribution is integrated over all angles. These theoretical assumptions are rarely completely and often not even approximately satisfied in experimental measurements. Therefore, it is of value to study these mixed distributions. This will be done here in a kind of semitheoretical approach.

The density distribution of cascade electrons can be expressed as a function of the projected coordinates defined in Fig. 3 by

$$g(r_1, r_2, \theta_1, \theta_2) dr_1 dr_2 d\theta_1 d\theta_2.$$

In general, this distribution should be a function of the linear sum of all possible combinations of the variables

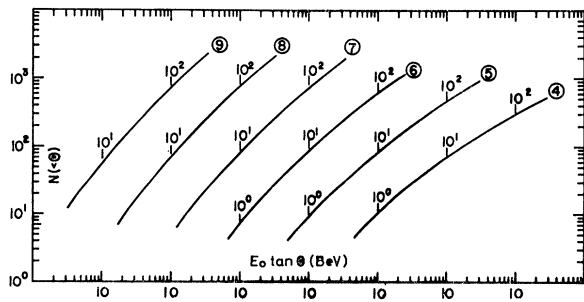


FIG. 2. Angular distribution of cascade electrons in the core approximation for an electron pair primary. The primary energy is in units of BeV and the angle Θ is in units of the tangent. The circles attached to the curves give the distance from the origin in radiation lengths. The curves are displaced horizontally, and the proper abscissa scale is indicated beside each curve.

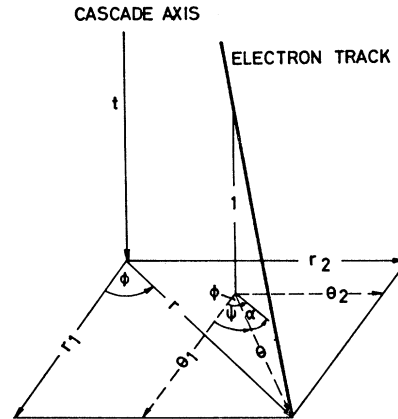


FIG. 3. Coordinate system indicating the relation between the various coordinates used for a sample track.

r_1, r_2, θ_1 , and θ_2 so that

$$g(r_1, r_2, \theta_1, \theta_2) dr_1 dr_2 d\theta_1 d\theta_2 = g(\chi^2) dr_1 dr_2 d\theta_1 d\theta_2, \quad (15)$$

where

$$\chi^2 = a\theta_1^2 + br_1\theta_1 + cr_1^2 + d\theta_2^2 + er_2\theta_2 + fr_2^2 + gr_2\theta_1 + hr_1\theta_2 + i\theta_1\theta_2 + jr_1r_2. \quad (16)$$

The space coordinates r and θ are related to the projected coordinates by

$$\begin{aligned} r_1 &= r \cos \phi, \\ r_2 &= r \sin \phi, \\ \theta_1 &= \theta \cos \psi, \\ \theta_2 &= \theta \sin \psi. \end{aligned} \quad (17)$$

with the angle ψ being related to the azimuthal angle ϕ and the angle α as defined in Fig. 3 by

$$\psi = \phi - \alpha. \quad (18)$$

Since a cascade exhibits cylindrical symmetry, the variable χ^2 must be independent of the azimuthal angle ϕ . Furthermore, a cascade should be symmetrical with respect to reflections through the cascade axis so that χ^2 is also independent of the sign of the angle α . With these restrictions, straightforward calculations show that the constants in Eq. (16) are such that

$$a=d, \quad b=e, \quad c=f, \quad g=h=i=j=0.$$

Therefore, χ^2 should be of the form

$$\chi^2 = a(\theta_1^2 + \theta_2^2) + b(r_1\theta_1 + r_2\theta_2) + c(r_1^2 + r_2^2). \quad (19)$$

If one normalizes the constants a, b , and c so that $a=1$, then χ^2 can be expressed as

$$\chi^2 = \theta_1^2 + \theta_2^2 + b(r_1\theta_1 + r_2\theta_2) + c(r_1^2 + r_2^2) \quad (20)$$

$$= \theta^2 + b\mathbf{r} \cdot \boldsymbol{\theta} + cr^2. \quad (21)$$

If χ^2 is indeed given by this expression, the differential angular and radial distributions of cascade electrons,

represented by $\Pi_1(\theta_1, \theta_2)d\theta_1d\theta_2$ and $\Pi_2(r_1, r_2)dr_1dr_2$, respectively, are given by

$$\Pi_1(\theta_1, \theta_2)d\theta_1d\theta_2 = d\theta_1d\theta_2 \int_{-\infty}^{\infty} dr_1 \int_{-\infty}^{\infty} dr_2 g(\chi^2), \quad (22)$$

and

$$\Pi_2(r_1, r_2)dr_1dr_2 = dr_1dr_2 \int_{-\infty}^{\infty} d\theta_1 \int_{-\infty}^{\infty} d\theta_2 g(\chi^2). \quad (23)$$

The integral distributions are then expressed by

$$N(<\Theta) = \int_0^{\Theta} \Pi_1(\theta) 2\pi\theta d\theta \quad (24)$$

and

$$N(<R) = \int_0^R \Pi_2(r) 2\pi r dr. \quad (25)$$

If, in the definition of χ given by Eq. (20), one makes the substitutions

$$\zeta_1 = \theta_1 + \frac{1}{2}br_1 = \zeta \cos \gamma$$

and

$$\zeta_2 = \theta_2 + \frac{1}{2}br_2 = \zeta \sin \gamma,$$

then the differential radial distribution expressed by Eq. (23) can be written as

$$\Pi_2(r) 2\pi r dr = 2\pi r dr \times 2\pi \int_{r(c-b^2/4)^{1/2}}^{\infty} \chi g(\chi^2) d\chi. \quad (26)$$

The central radial density, i.e., $\Pi_2(r \rightarrow 0)$, is given by

$$\Pi_2(r \rightarrow 0) = 2\pi \int_0^{\infty} \chi g(\chi^2) d\chi. \quad (27)$$

Consequently, the value of $\Pi_2(r)$ at any r is expressed by

$$\Pi_2(r) = \Pi_2(r \rightarrow 0) - 2\pi \int_0^{r(c-b^2/4)^{1/2}} \chi g(\chi^2) d\chi. \quad (28)$$

Analogously, the differential angular distribution can be expressed as

$$\Pi_1(\theta) 2\pi\theta d\theta = 2\pi\theta d\theta (2\pi/c) \int_{\theta(1-b^2/4c)^{1/2}}^{\infty} \chi g(\chi^2) d\chi, \quad (29)$$

with the central angular density being

$$\Pi_1(\theta \rightarrow 0) = (2\pi/c) \int_0^{\infty} \chi g(\chi^2) d\chi. \quad (30)$$

Therefore, the value of $\Pi_1(\theta)$ for any θ is given by

$$\Pi_1(\theta) = \Pi_1(\theta \rightarrow 0) - (2\pi/c) \int_0^{\theta(1-b^2/4c)^{1/2}} \chi g(\chi^2) d\chi. \quad (31)$$

Since $\Pi_1(\theta \rightarrow 0) = (1/c)\Pi_2(r \rightarrow 0)$, as expressed by Eqs. (27) and (30), it follows from Eqs. (28) and (31)

$$\Pi_1(\theta = c^{1/2}r) = (1/c)\Pi_2(r). \quad (32)$$

Consequently, the integral radial and angular distributions are correlated by

$$N(<R) = N(<\Theta = c^{1/2}R). \quad (33)$$

In other words, the integral-radial and integral-angular distributions are identical except for a shift in scale which is given by $\theta = c^{1/2}r$. Indeed, by comparing the theoretical calculations for the radial and angular distributions, one finds that they can be made to coincide quite well by a horizontal shift in the R or Θ scale, over the ranges of r and θ investigated here.

The shift in scale between the integral radial and angular distribution determines uniquely the parameter c . Since $g(\chi^2)$ is a monotonic function of χ , the parameter b can be determined according to Eq. (21) from the relation

$$\theta_{\max} = -\frac{1}{2}br,$$

where θ_{\max} is the angle at which the maximum occurs in the density of particles having the angle $\alpha=0$ for fixed values of r . In principle, therefore, the parameter χ can be uniquely determined experimentally.

The great value of this approach becomes now apparent. What has been done here is not only a study of the mixed radial-angular distribution.

Experimentally, values of the function $g(\chi^2)$ have been measured over a domain of χ that is much larger than would have been possible to achieve by a measurement of radius or angle alone. The method discussed here provides therefore a technique of extrapolation from the measured density values at ranges of the variables $r_1 r_2 \theta_1 \theta_2$ that can be covered by our measuring technique to density values that belong to variables that we can not cover.

In other words, the assumption Eq. (21) tells us what density of electrons to insert at values $r_1' r_2' \theta_1' \theta_2'$ outside our measurement range, namely the same density as that measured for values $r_1 r_2 \theta_1 \theta_2$ inside our measurement range, where

$$\theta'^2 + br' \cdot \theta' + cr'^2 = \chi^2 = \theta^2 + br \cdot \theta + cr^2.$$

Thus, by this method, the range covered by the variables can be extended in a rational manner.

The question remains open as to whether the particular assumption made in Eq. (21) is justified. We will discuss this point in Sec. V.

III. MEASUREMENTS

Simultaneous measurements of the position and angular orientation have been made for each cascade electron in ten high-energy electromagnetic cascades which were initiated by single γ rays. Six of these cascades were developed in the Brawley pure-emulsion

stack.¹³ This stack consisted of 500 sheets of Ilford K-5 nuclear emulsion (1 r.l. = 28.3 mm), each having the dimensions $45 \times 60 \times 0.06$ cm³. This stack was launched with a balloon from Brawley, Calif., in 1961 and was recovered after having flown approximately 30 h.

In addition to the cascades from the Brawley stack, four cascades were measured in emulsion plates which were borrowed from the Institute of Nuclear Research in Krakow, Poland. These plates were part of the SSS lead-emulsion sandwich stack which was irradiated at balloon altitude for about 5 h in Italy in 1961.¹⁴ The SSS stack consisted of 140 Ilford G-5 nuclear emulsion plates each having dimensions $25 \times 25 \times 0.06$ cm³ and 70 lead plates each 2 mm thick. The stack was constructed so that two emulsion plates were placed between adjacent lead plates. The radiation length of the stack was calculated to be 8.1 mm by assuming a homogeneous mixture of lead and emulsion.

Since the distance from the cascade origin can only be measured with certainty from the first electron pair, the initiating γ rays were required to have materialized inside the stack. To insure that the cascade-initiating particle was indeed a single γ ray, the Brawley cascades were required to fulfill the following criteria:

- (1) The origin of the first pair was located within about two conversion lengths from the edge of the stack.
- (2) The origin of the first pair was found and scanning of the adjacent area showed no accompanying parallel tracks which might be connected with a low-multiplicity nuclear interaction.
- (3) The origin of the first bremsstrahlung pair was located a reasonable longitudinal distance from the origin of the primary pair (~ 1 cm) and had a small lateral displacement from that pair ($< 3 \mu$).
- (4) The cascade had only one apparent core.
- (5) Scanning of the immediate area around the cascade showed no secondary interactions.

The cascades in the SSS lead-emulsion sandwich stack could not be continually observed throughout their development since much of the development was in the lead plates. Consequently, all of the above criteria could not always be used for this stack. For example, the first emulsion plate through which a cascade passed after entering the stack was scanned for accompanying parallel tracks in lieu of criterion 2. Also each of the SSS cascades was traced throughout each emulsion plate in which it could be found. These observations showed that each cascade had only one apparent core. When the cascade origin could not be found in an emulsion plate, calculations were performed by using the dip angle of the cascade to locate the origin within a lead plate. To calculate the distance t from the origin where measurements were made, the origin was assumed to

¹³ F. Abraham, J. Gierula, R. Levi Setti, K. Rybicki, C. H. Tsao, W. Wolter, R. L. Fricken, and R. W. Huggett, *Phys. Rev.* **159**, 1110 (1967).

¹⁴ J. Babecki, R. Holynski, S. Krzywdzinski, A. Peeva, K. Rybicki, and W. Wolter, *Nucleonika* **9**, 271 (1964).

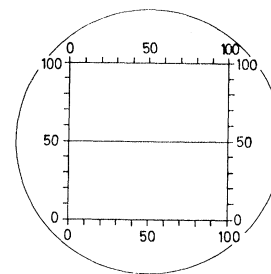


FIG. 4. Schematic diagram of the box graticule as it appeared in the field of view of the Koristka R4 microscope.

be in the center of this lead plate. By calculating the distance traveled in each lead and each emulsion plate from the dip angle of the cascade, the distance t in radiation lengths was calculated using 5.7 mm/r.l. for lead and 28.3 mm/r.l. for emulsion.

Measurements were made on each Brawley cascade at distances t from the origin which corresponded to 5, 7, and 9 r.l. The positions of measurements on the SSS cascades were restricted by the development of the cascades in the lead plates, but these SSS cascades were also measured as closely as possible to 5, 7, and 9 r.l.

The actual measurements were performed by using a Koristka R4 microscope which has a vernier scale to permit determination of the depth of the field of measurement in the emulsion relative to the emulsion surfaces. The position and angle of all cascade tracks were measured over a lateral spread of $\gtrsim 600 \mu$ to either side of the apparent cascade core. This was accomplished by placing a square "box" graticule in the eyepiece of the microscope. Each side of the graticule was marked off into 100 scale divisions (see Fig. 4). The graticule also contained a bisecting centerline which was oriented perpendicular to the cascade core and this centerline was taken to be the position of the target plane for the measurements at a specific distance from the cascade origin. The graticule covered a square area in the emulsion of approximately 85μ per side under the magnification used ($10 \times$ eyepieces with $55 \times$ objective). Therefore, in order to measure the desired lateral spread, it was necessary to measure the tracks in 15 adjacent volumes, $85 \times 85 \times 600 \mu^3$, with the cascade core located midway between the glass and air surfaces of the emulsion in the center volume. Each track, which had grain density around the plateau value for singly charged particles, that crossed the horizontal centerline of the graticule was traced to the two points where it intersected the sides of the graticule. Tracks having twice the grain density of singly charged particles were considered to be an electron-positron pair and were recorded as two particles. The particular graticule sides and the corresponding scale readings at the intersections of the track with those sides of the graticule were recorded along with the relative positions of the measuring field in the emulsion. These data were punched on cards and subsequent analysis was performed with an IBM 7040 computer to obtain the spatial position

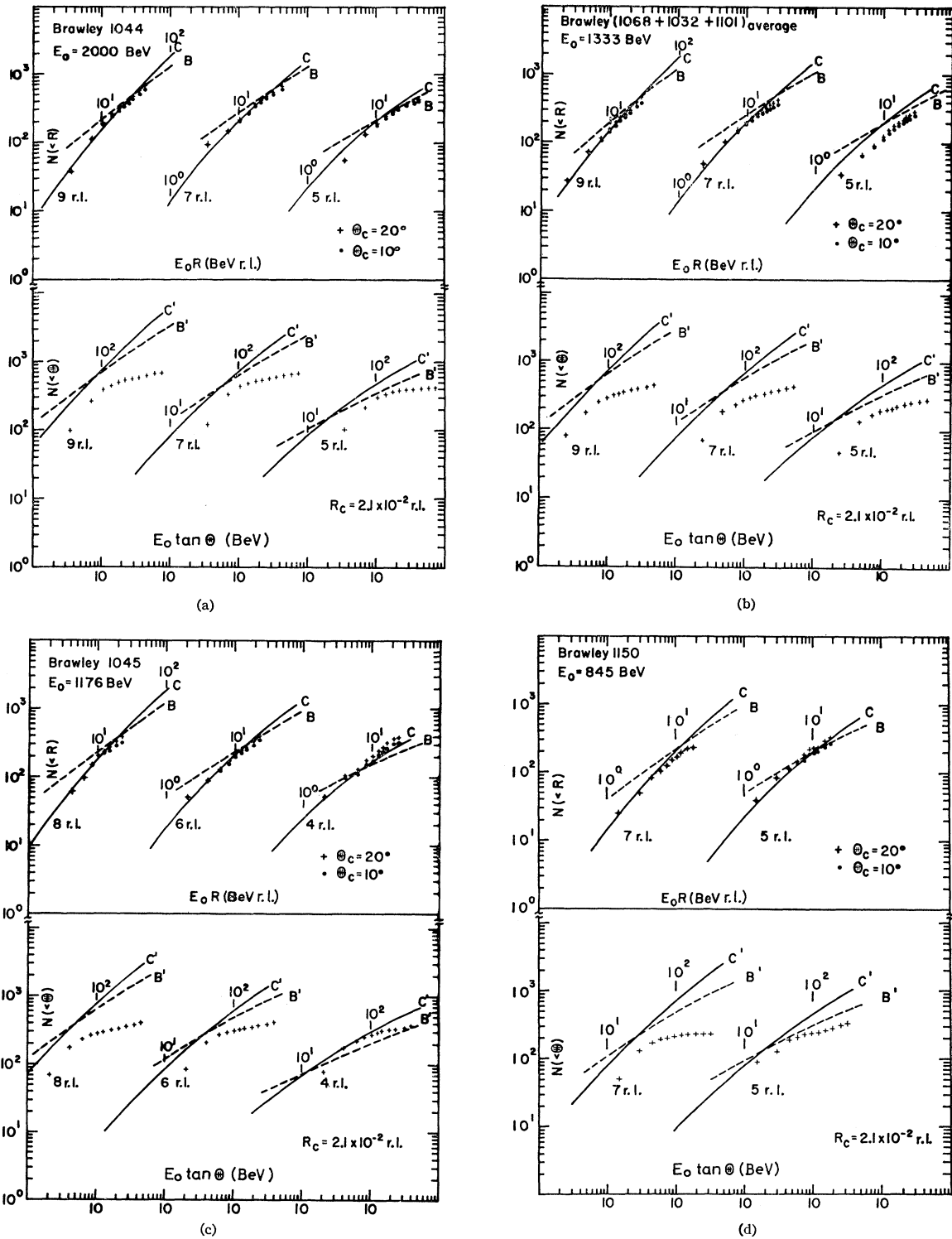


FIG. 5. Radial and angular distributions of the electrons in the measured cascades. Parts (a)-(g) are for different cascades, which are identified by the cascade number and the primary energy. The distance l from the cascade origin is given below the curves while the scale for the abscissa is indicated beside the curves. The curves are displaced horizontally. The top half compares the integral number of electrons $N(<R)$ with the radial-core approximation (curve C) and approximation B (curve B). Experimental points are given for cutoff angles $\Theta_c = 10$ and 20 deg. The bottom half compares the integral number of electrons $N(<\Theta)$ with the angular-core approximation (curve C') and approximation B (curve B'). Experimental points are given for the radial cutoff $R_c = 2.1 \times 10^{-2}$ r.l. and for the SSS cascades also at 7.4×10^{-2} r.l.

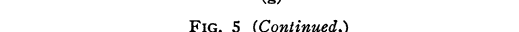
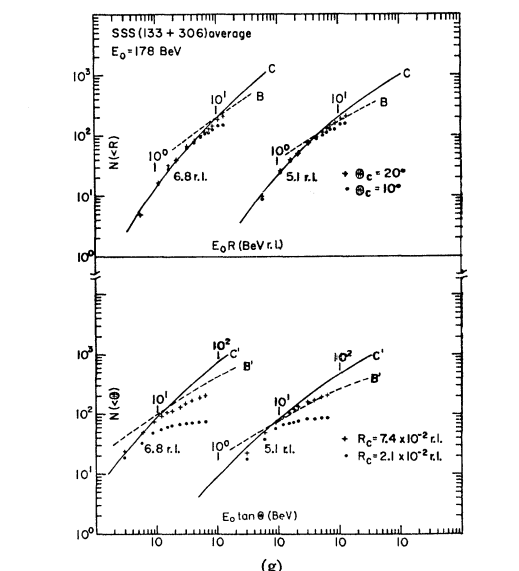
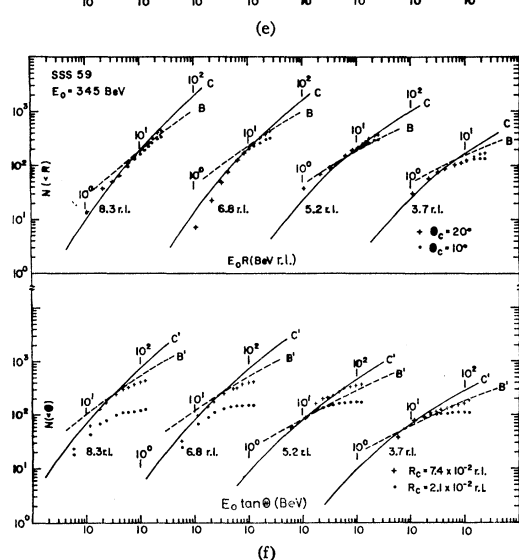
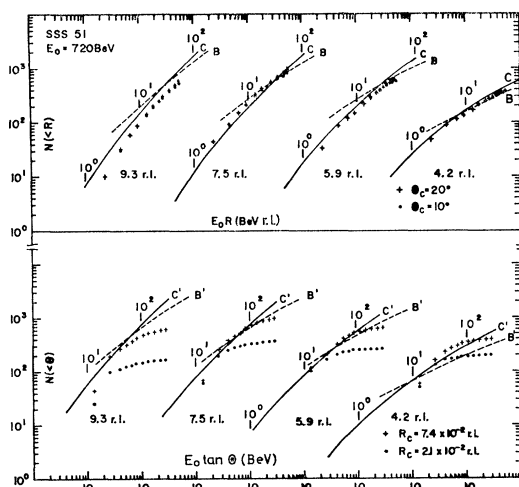


FIG. 5 (Continued.)

and angular orientation of each particle relative to the cascade axis. See Fig. 3 for definitions of the coordinates used.

The cascade axis was determined by requiring the average values of the coordinates (both position and angle) to be zero, i.e., $\bar{r}_1=0, \bar{r}_2=0, \bar{\theta}_1=0, \text{ and } \bar{\theta}_2=0$. The average values of the respective coordinates were obtained by an iterative method of successive approximations. Only those tracks which had both a lateral separation of less than 250μ from the cascade core and which made an angle less than 5° with respect to the direction of the core as measured on the microscope were used in the iteration. The first approximation to the average value of any particular coordinate was obtained by a simple average over that coordinate for all tracks which satisfied the above criteria. Subsequent iterations for the average value of that coordinate (say r) were given by

$$\bar{r}_{i+1} = - \frac{1}{n} \sum_{j=1}^n (r_j - \bar{r}_i), \quad (34)$$

where n was the 75% of the tracks which had the coordinate r_j closest to the previous mean \bar{r}_i . The iteration was stopped when

$$|\bar{r}_{i+1} - \bar{r}_i| < \epsilon_r,$$

where ϵ_r was taken to be 0.5μ for the lateral coordinates and 0.001 rad for the angular coordinates.

All cascade tracks, irrespective of angle, were measured over a lateral spread of $\geq 600 \mu$ to either side of the cascade core. Since the undeveloped emulsion was approximately 600μ thick, these lateral measurements extended to about twice as far from the core as the respective glass and air surfaces of the emulsion. Thus, while one could obtain exact distributions of the track coordinates up to distances of about 300μ from the cascade axis, larger distances required some correction. The needed correction was calculated from the ratio of the area in that part of an annular ring (centered about the cascade axis) in which measurements were made to the entire area of the ring. The technique amounts to assuming aximutal symmetry of particles around the cascade axis.

Since the cascade measurements were performed on the tracks of all singly charged particles in the measuring volume, many particles which were not actual cascade electrons were necessarily measured. These additional particles which consist of protons, mesons, muons, etc., are called "background." In order to determine the background level, exactly the same measurements as were made for the cascades were performed in several volumes of the emulsion which were located ≥ 1 cm from the core of the cascades.

The same calculations were performed on the background tracks as was done for the data consisting of cascade tracks superimposed on background with the exception of the background "axis." The coordinates of

TABLE II. Cascade energies using core approximation.

Cascade		E_0 (BeV) from radial distribution	E_0 (BeV) from angular distribution
Brawley (1068, 1032, 1101)average	1044	2000	...
	1045	1333	...
	1150	1176	...
		845	...
SSS (133, 306)average	51	720	780
	59	345	333
		178	174

each track in the background data were calculated relative to an axis perpendicular to the horizontal centerline of the box graticule, i.e., parallel to the cascade core direction. Since the axis of each cascade was inclined at some angle (dip angle) with respect to the emulsion surface, the background track coordinates were also calculated relative to several axes inclined at different angles. The dip angle of the background axis could then be matched with the axis of any cascade. Therefore, for any distribution of coordinates which was desired, the corrections for background noise could be made by a simple subtraction of the average background from the distributions of the cascade superimposed on background.

IV. RESULTS

From the initial cascade measurements the projected coordinates r_1 , r_2 , θ_1 , and θ_2 of each electron in the cascade were determined for the coordinate system having the t axis coincident with the cascade axis. The space coordinates r and θ , which give, respectively, the lateral displacement and angular orientation of each track relative to the cascade axis, were calculated from the projected coordinates. At each position of measurement, the integral radial and integral angular distributions were then determined. The integral radial distribution specifies the number of particles, irrespective of angle, contained within a circle of radius R centered about the cascade axis. The integral angular distribution gives the number of particles having angles less than Θ without regard to lateral position.

The primary energy E_0 of each cascade was determined from the radial distribution by comparing the experimental points with the core approximation curves. Only the experimental points within $\sim 10^{-2}$ r.l. of the cascade axis were taken into consideration, since this is the region where the core-approximation curves had previously been shown to be reliable.

In making the comparison, a transparent overlay containing the core-approximation curves $N(<R)$ versus E_0R plotted to the same scale as the experimental points was simultaneously fitted by eye to the experimental distributions $N(<R)$ versus R at all the measured depths from the origin for an individual cascade. The

matching of the curves in this manner is done with some ambiguity. However, the agreement in the energy estimation by two different observers was better than 95%. The radiation lengths near the maximum of the longitudinal development ($\sim 6-7$ r.l.) were given the largest weight, since these should have the smallest fluctuations. The primary energy of the cascade was then given by the ratio of the E_0R scale of the core-approximation curves to the R scale of the experimental distributions. The energies of the cascades as determined from the radial distributions are shown in column 2 of Table II.

The experimental radial and angular distributions of the cascades are compared with the theoretical predictions of the core approximation and approximation B in Fig. 5(a-g). The top half of each figure displays the number of cascade particles $N(<R)$ having lateral displacements less than R from the cascade axis as a function of E_0R , and the bottom half shows the number of cascade particles $N(<\Theta)$ having angles less than Θ with respect to the cascade axis as a function of $E_0 \tan \Theta$. The curves for the radial-core approximation (curves C) were taken from Kidd,⁹ while the curves for the angular-core approximation (curves C') were taken from the calculations presented in Sec. II B. The curves of approximation B for the radial distribution (curves B) and the angular distribution (curves B') were calculated by determining the total number of particles from Fig. 5.13.3

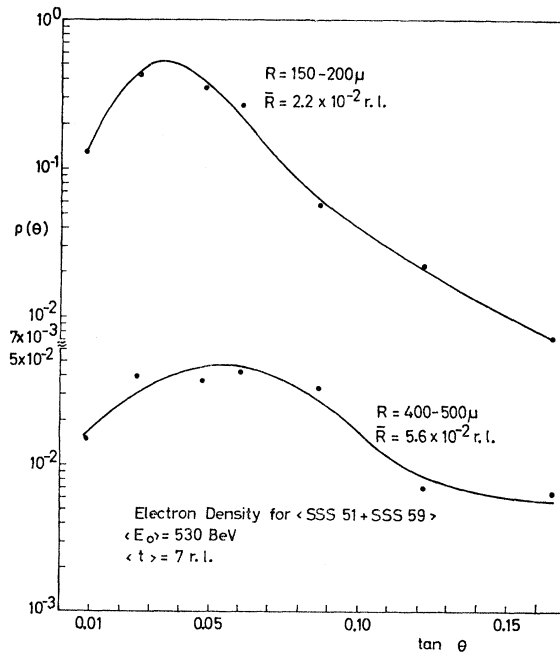


Fig. 6. Density distribution $\rho(\theta)$ versus θ of the electrons having the angle $|\alpha| \leq 20$ deg and located within the annular rings defined by the radial displacement $150\mu < r \leq 200\mu$ and $400\mu < r \leq 500\mu$. These are example distributions from the average of cascades SSS 51 and SSS 59 given to indicate the displacement in position and width of the maximum at different distances from the cascade axis. The curves were obtained by a least-squares fit to the data points.

of Rossi¹² and using the normalized radial and angular distributions given, respectively, by Fig. 7 of Pinkau³ and the present authors' Sec. II A.

Brawley cascades 1068, 1032, and 1101 had approximately the same energies. Therefore, in order to decrease fluctuations, the distributions of these cascades were averaged and are presented in the figures as one cascade. For the same reason, SSS cascades 133 and 306 are presented as a single cascade.

For statistical reasons, we have also combined the electron number distributions for cascade SSS 51 at $t=5.9, 7.5,$ and 9.3 r.l. with the distributions of SSS 59 at $t=5.2, 6.8,$ and 8.3 r.l. The resulting data were averaged and then considered as representing a single cascade having primary energy equal to the average of the two cascades, i.e., 530 BeV, at the depth from the cascade origin equal to the average of the individual depths, i.e., $t=7$ r.l. It is this average which is considered below in making comparison with the calculations presented in Sec. II C for the mixed radial-angular distribution.

The parameters b and c used in the definition of χ were calculated according to the argument given in Sec. II C to be -2.04 and 4.41 , respectively. The value of c was found to be the same whether the theoretical or the experimental integral distributions were considered and is believed to be sufficiently accurately determined. In the determination of b we have used those particles which have the angle $|\alpha| \leq 20$ deg in finding the particle density distribution $\rho(\theta)$ versus θ for various fixed values of r . For $r < 150 \mu$, this distribution was maximum at angles on the order of our experimental accuracy (~ 1 deg). Therefore, the value of b was taken to be the average obtained from the position of the maximum in the density distributions at larger values of r . The maximum was determined in each case by a least-squares fit to the data points which had an average over-all standard

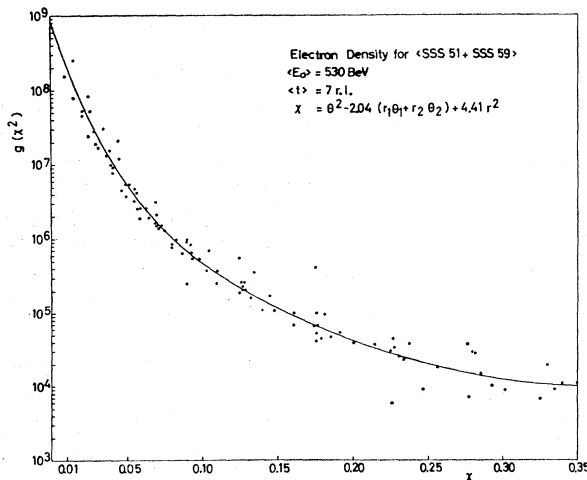


FIG. 7. Density distribution $g(\chi^2)$ versus χ for the average of cascades SSS 51 and SSS 59. The curve represents a least-squares fit to the data points with an over-all standard deviation of 21%.

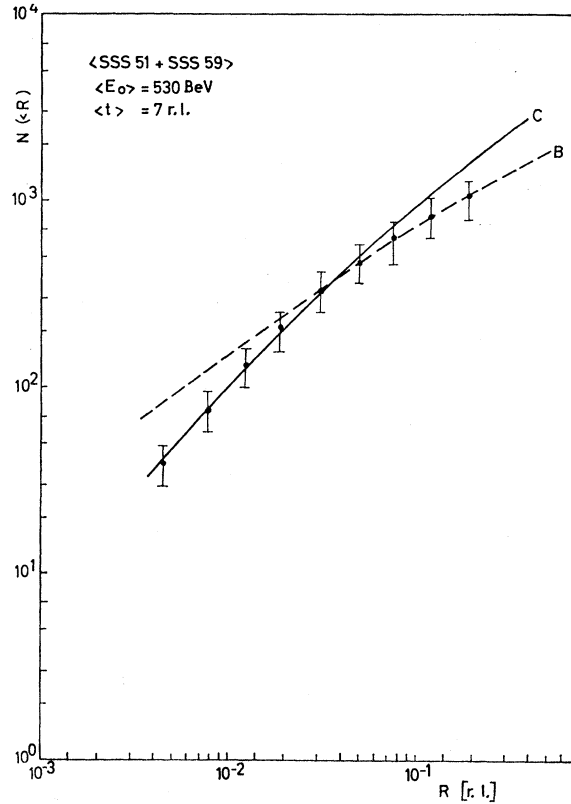


FIG. 8. Integral radial distribution as calculated from the mixed radial-angular distribution, i.e., from Fig. 7. Comparison is made with the core approximation (curve C) and approximation B (curve B). An arbitrary error of 25% has been attached to the points.

deviation of 5%. Two typical examples of the angular-density distribution are shown in Fig. 6. These examples show the shift in the position of the maximum as the radial distance is increased. They also indicate the increased width of the distribution about the maximum and the decrease in statistical accuracy for the larger distances from the cascade axis.

With b and c determined, the parameter χ was calculated for each cascade particle, and subsequently the function $g(\chi^2)$ versus χ also was determined by a least-squares fit with an over-all standard deviation of 21%. This function is shown with the experimental points in Fig. 7 up to values of $\chi=0.35$.

The central radial density $\Pi_2(r \rightarrow 0)$ could not be directly calculated as given in Eq. (27), since we have not measured χ indefinitely. However, the central density $\Pi_2(r \rightarrow 0)$ is of course known experimentally, since it is completely within the domain covered by our measurements. In order to determine $\Pi_2(r \rightarrow 0)$ one would however have to extrapolate back to $r \rightarrow 0$. Therefore, one may rather use a generalization of Eq. (28), namely,

$$\Pi_2(r) = \Pi_2(r_s) - 2\pi \int_{r_s(c-b^2/4)^{1/2}}^{r(c-b^2/4)^{1/2}} \chi g(\chi^2) d\chi \quad (35)$$

for $r > r_s$. Now, r_s is a certain small value of r which is chosen such that $\Pi_s(r_s)$ can be completely and safely determined from our experimental results. For the value of r_s , 50μ has been used.

In this manner, it was still possible to determine the central density. However, our main interest has been in establishing the electron density at large values of r , and the central density was of interest chiefly for the sake of consistency.

In Fig. 8, the integral radial distribution as calculated from the mixed radial-angular distribution, i.e., from $g(\chi^2)$ versus χ , where $\chi^2 = \theta^2 - 2.04 (r_1\theta_1 + r_2\theta_2) + 4.41r^2$, is compared with the theoretical curves predicted by both the core approximation and approximation B. An arbitrary error of 25% has been attached to the points. These calculated points extend up to $R = 1.9 \times 10^{-1}$ r.l. ($\chi = 0.35$), whereas the directly measured points extended up to $R = 7.4 \times 10^{-2}$ r.l. In other words, the radial domain has been extended by a factor of about 2.5.

We are able to extrapolate our measurements beyond the radial domain actually measured as long as we keep inside $\chi = 0.35$ for which some experimental results exist. Of course, our method of extrapolation depends on the assumption of the validity of Eq. (20). That this assumption is valid is substantiated by the fact that the theoretical and experimental $N(E_0R)$ and $N(E_0 \tan\Theta)$ distributions can be made to coincide by multiplying the variables with one factor, i.e., by satisfying the relation Eq. (33).

V. DISCUSSION

The comparisons shown in the top half of Fig. 5 (a-g) of the directly measured experimental radial distributions with the theoretical curves of the core approximation and approximation B indicate that the experimental results are generally consistent with the cascade theory under the core approximation in the radial and energy range which were measured. The measurements in the Brawley stack extended up to $R = 2.1 \times 10^{-2}$ r.l. and covered an energy range of 845–2000 BeV, while in the SSS stack the radial measurements were made up to $R = 7.4 \times 10^{-2}$ r.l. and the energy range was 178–720 BeV.

As shown in the bottom half of Fig. 5(a-d) there is an apparent discrepancy when the angular distributions of cascade particles measured in the Brawley stack are plotted as a function of $E_0 \tan\Theta$ and compared with the cascade theory under the angular-core approximation. This apparent discrepancy could conceivably stem from two sources. The first source could be an internal inconsistency in the predictions of the theoretical curves while the second could be that the measurements suffered from the limited radius (2.1×10^{-2} r.l.) which was covered in the Brawley stack. From the measurements in the SSS stack where the radial range was much larger (7.4×10^{-2} r.l.), it is clear that the latter source is the

correct one. The bottom half of Fig. 5 (e-g) shows that for the SSS stack, the radial cutoff $R_c = 2.1 \times 10^{-2}$ r.l. does not allow the measurement of all particles even at 1–2 deg. However, for $R_c = 7.4 \times 10^{-2}$ r.l., there is good agreement of the experimental points up to ~ 4 –5 deg with the cascade theory under the core approximation. Consequently, one must conclude that no comparison is possible between theory and experiment for the angular distributions in the Brawley stack, because the limited radial interval which could be measured did not permit the measurement of all particles even at very small angles.

The deviation of the experimental angular distribution from the core approximation for angles greater than ~ 4 –5 deg in the SSS stack can certainly be explained to some extent by the fact that the radial limitation of 7.4×10^{-2} r.l. was not large enough to include all particles having angles greater than 5 deg. This appears to be a major reason for the apparent deviation, but it does not exclude the possibility that part of this deviation may truly be a deviation from the core approximation.

Indeed, as shown in Fig. 8, the radial distribution determined from the mixed radial-angular distribution according to the argument presented in Sec. II C clearly indicates that the true electron distribution deviates from the core approximation curve and begins to follow the curve of approximation B. Furthermore, this transition occurs near the predicted intersection of the two approximations. This implies not only that the range of the core approximation has been reached, but also that approximation B correctly represents the cascade distributions for larger distances from the cascade axis.

We want to emphasize that the radial distribution shown in Fig. 8 represents the average of two cascades at six different positions of measurement. This average was deemed necessary in order to have sufficient statistics for the calculation of the parameter χ used in determining the density distribution. That this average is capable of representing an individual measurement on a cascade is substantiated by the fact that the directly measured average distribution follows the curve for the core approximation in its previously shown range of validity. The extrapolation of our results is therefore dependent only on the validity of Eq. (20) and the accuracy with which the parameter χ , i.e., Eq. (35), can be determined. The agreement of the calculated distribution with the core approximation in its previously shown range of validity indicates that Eq. (35) is sufficiently accurate.

The final point that requires discussion is the assumption made in Eqs. (15) and (21) about the particular choice of the form of the density distribution function.

We have convinced ourselves experimentally that the density of electrons is really a function of the variable χ as defined in Eq. (21). This is illustrated, for example, in Fig. 9, in which the density of electrons is shown to

remain constant if one varies r and only χ is kept constant.

We believe, therefore, that our extrapolation method is applicable because this functional behavior of χ is not expected to change drastically.

Another piece of evidence is that quoted in Sec. II C, namely the coincidence of the distributions $N(<R)$ and $N(<\Theta=c^{1/2}R)$ over our range of variables.

The functional behavior of Eq. (21) is also that of multiple-scattering theory without energy loss given by Rossi.¹² One should therefore expect that Eq. (21) has also only a limited domain of applicability, namely that in which most of the electrons have energies larger than the critical energy (ϵ_0). One must not be disturbed here by the agreement with the theoretical distribution derived "under approximation B," since this is really in the first place, an "approximation for large radii." This has extensively been discussed previously³ and need not be repeated here. Essentially, the electrons will deviate from the "core approximation" and follow the "approximation for large radii" while they still have energies in excess of ϵ_0 . This allows us to apply Eq. (21). If one goes still further away from the cascade core, the average electron energy will become comparable to ϵ_0 , and Eq. (21) is then expected not to hold any more.

It should also be noted that, in exact analogy to the use of the radial distributions, the primary energy of the SSS cascades can be determined by considering only the experimental points for the angles where all particles have been measured, and making direct comparison with the theoretical curves obtained under the angular core approximation that are given in Sec. II B. The results of the energies so obtained are given in column 3 of Table II. One can see that there is good agreement between the energy estimates obtained from

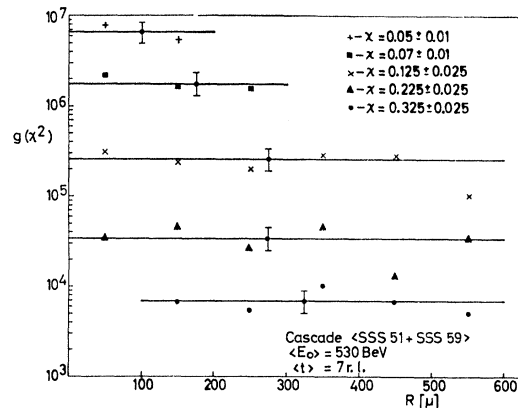


FIG. 9. The function $g(\chi^2)$ versus R with χ as a parameter. This figure indicates that within the range of our measurements the electron density $g(\chi^2)$ is only a function of the parameter χ , i.e., $g(\chi^2)$ is independent of the radial distance from the cascade axis. The experimental points were calculated for the χ intervals indicated within radial increments of 100μ and are plotted at the midpoint of these intervals. The solid curves are a simple average of the data points and are shown with an arbitrary error of 25%. These solid lines do not necessarily have exactly the same density magnitude as that given in Fig. 7 since the latter was determined by a least-squares fit to all our data points, which were weighted equally.

the radial and angular distributions. Two obvious conclusions can be drawn from this agreement in energy determination. First, it shows the internal consistency of the cascade theory as derived under the core approximation. Second, it indicates that the sandwich arrangement of the heavy SSS stack is sufficiently fine so that it can be considered to be a homogeneous mixture of lead and emulsion as far as the determination of the effective radiation length for the radial distribution is concerned.